IJPGC 2003
2003 International Joint Power Generation Conference
June 16-19, 2003, Atlanta, Georgia, USA

IJPGC2003-40058

COUPLED CFD AND THERMAL STEADY STATE ANALYSIS OF STEAM TURBINE SECONDARY FLOW PATH

Leonid Moroz , SoftInWay Inc. **Alexander Tarasov , SoftInWay Inc.**

ABSTRACT

The main purpose of this work is to conduct coupled CFD analysis of the steam flow in the secondary part of turbine and study thermal rotor/stator steady state.

We consider a 11 stage high-pressure cylinder of a power steam turbine with extended terminal labyrinths. Domain of interest is only the secondary flow path of the cylinder, therefore the shroud and blades are beyond the scope of this work. All blades are virtually removed and on the imaginary cylindrical surface the effective boundary conditions are assigned. This takes into account heat fluxes that came to disks/diaphragms from blades in reality.

Practical engineering method of obtaining axi-symmetric solution has been developed and results are presented and discussed. Thermal state analysis shows a significant influence of secondary steam bleeding on temperature distribution of rotor and stator.

INTRODUCTION

Prediction of steam turbine rotor and stator thermal state is a complex problem that usually is divided into a set of interdependent problems related to steam flow, heat transfer and thermo-mechanical modeling. Some of most important modeling issues can be identified as follows:

- Turbine flow path heat transfer boundary conditions;
- Heat transfer boundary conditions related to the secondary part;
- Secondary steam flow including the flow in disk/diaphragm cavities and seals;
- Windage losses;
- Turbine rotor and stator thermal steady analysis;
- Seals radial/axial clearance optimization.

The most reasonable and correct way to solve the problem is a coupled solution when all boundary conditions and thermal state of turbine parts are interactively evaluated. Usually, all mentioned tasks are addressed separately due to obvious difficulties of computation. This typical approach lacks accuracy since temperature of the secondary steam with relatively small mass flow rate is changing significantly through the secondary part channels. Meanwhile, the steam temperature computation can be easily made more precise and close to real conditions by successive iterative calculations of both solid thermal state and steam-solid heat exchange. Thus, the key to the problem is the secondary steam flow prediction, which, as a rule, is obtained with the help of network model that includes labyrinth seals, disk's balance holes, cavities between disk and shroud, etc. This approach not always adequately reflects the process because the network model is based on a simplified concept of flow behavior in disk cavities and in some cases usage of such model could lead to significant errors. Therefore, a CFD analysis is more preferable way for obtaining the solution. Numerous studies of rotated disk-stator system have been carried out using CFD approach (see, for example, Wilson, Pilbrow, Owen, 1997-1999 and Kapinos, Matveev, Pustovalov, 1983). All these studies contain theoretical and experimental analyses that show very intricate phenomena of flow and heat transfer in such kind of systems. Vortexes in the terminal parts of cavities, pumping effect, mixing in balance holes are only a few phenomena that can't be accurately predicted by a simple model based on idea of boundary layers on disk and stator surfaces. Unfortunately, the majority of published CFD works is restricted to the gas turbines. The present work is an attempt to fill the void in secondary flow analysis for steam turbines using the new method developed by authors.

NOMENCLATURE

p – pressure
v – specific volume
T – temperature

G – mass flow rate
μ, φ – flow rate factor
D – diameter of labyrinth seal
d – diameter of balance holes
δ – labyrinth seal clearance
z – number of knifes in labyrinth seal or balance holes
$u_{\theta w}$ – shaft rotational velocity
$\beta = \dfrac{\overline{u}_\theta}{u_{\theta w}}$ - relative velocity of fluid (swirl factor)
Nu – Nusselt number
Re – Reynolds number
Pr – Prandtl number

Indexes:
in – inlet of hyper-element channel
out – outlet of hyper-element channel

1 Modeling of the Rotor and Diaphragms

The domain of interest of this work is a rotor/stator system of a large steam turbine with entry steam pressure 23.5 MPa and temperature 810 K. Considered here high-pressure cylinder possesses by all typical design features of steam turbine. The thermal state model of 11 stages rotor/stator with long shaft terminal zones is considered. It includes fluid zones in 22 stator/rotor cavities, 11 diaphragms, 7 balance holes per disk and terminal labyrinth seals. All these elements form the steam secondary flow system.

1.1 Thermal Boundary Conditions

Because turbine main flow path is not the object of interest, the blades and vanes are not explicitly modeled. Their thermal influence on diaphragm and disk surfaces is taken into account by equivalent boundary conditions, including heat fluxes from blades and end surfaces of turbine passages.

1.2 Flow Boundary Conditions

Flow pattern in disk cavity significantly depends on main and secondary steam flows interaction in near-root zone (see Phadke, Owen, 1988). Due to this fact, for more correct modeling of main/secondary steam flows interaction, the fluid zones are extended at the expense of virtual fields inside flow path (Fig.1). Pre-computation was performed to define dimensions of a zone projected into flow path. Dimensions of that zone assumed optimal if boundaries influence on a flow pattern in the zone was negligible.

Axial and swirl velocity components and steam static temperature are assigned at zone inlet, while static pressure and steam full temperature are assigned at outlet. Mentioned parameters correspond to exit steam parameters in blades near-root zone. Slip condition is applied for upper bound.

It is obvious that obtained results for projected zone don't completely describe the steam flow pattern in near-root zone because they do not include blades and vanes influence on the flow. Nevertheless, such approach allows to quite correctly include the interaction of main and secondary flows.

Conditions for joint boundaries of disk-stator cavity with labyrinth seal and balance hole are assigned as controlled boundary conditions

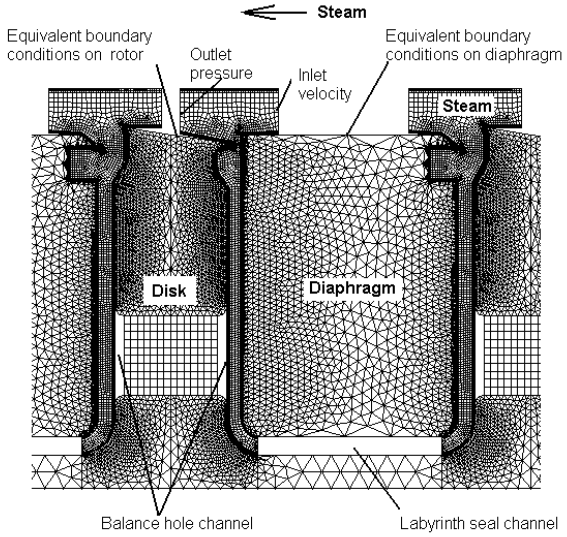

Fig. 1 Fragment of the fluid-solid model for coupled analysis of thermal state of secondary flow in the high-pressure cylinder of large steam turbine

.

2 Controlled Boundary Conditions - CFD Extension

Basically, existing CFD packages allow solving the presented problem as a directly coupled solution. However, the direct solution requires such unmanageable mesh that it makes the task practically unrealizable. The mesh analysis shows that the finest mesh is usually located in the field with the small items of diaphragms and terminal labyrinth seals and almost completely absorbs all computer resources.

At the same time, main flow features are located in the disk/stator cavities and can't be adequately addressed with the simplified model. Furthermore, such elements like balance holes require 3D modeling instead of more convenient axi-symmetric one.

To avoid these difficulties, the more innovative method was developed based on idea of controlled boundary conditions for separated fluid fields during the CFD solver iterations. Method consists of the following steps. Zones of labyrinth seals are extracted from total fluid domain of the secondary steam flow and the hyper-elements linked to the rest of the model are embedded in general scheme of CFD formulation. Besides that, the balance holes are also considered as embedded linked hyper-elements. As a result, the disk mesh doesn't include balance holes and this reduces the problem to axi-symmetric one.

After these steps the fluid mesh looks like several separated disk/stator cavities channeled by hyper-elements. Flow rate from one separated field into another, as well as, heat transfer and heat generation in the elements are described by experimental correlations.

The correlation for labyrinth seal can be presented as:

$$G = \mu\pi D\delta\sqrt{\frac{p_{in}^2 - p_{out}^2}{zp_{in}v_{in}}}, \qquad (1)$$

where the rate factor μ reliably determines design specifics.

Flow rate through the balance hole is defined by the following formula:

$$G = \varphi\frac{\pi d^2}{4}z\sqrt{2\frac{p_{in} - p_{out}}{v_{in}}}, \qquad (2)$$

Flow rate factor for balance hole depends on the disk rotational velocity, steam velocity in the balance hole, holes diameter, radius of the holes location on the disk, and fillets radius. φ-factor was determined from tabulated experimental nomograms.

CFD solver provides entry P_{in} and exit P_{out} pressure. Both values are extracted for each iteration in order to determine the flow rate using correlations (1, 2). The results of computation are applied as the boundary conditions on inlet and outlet faces of the hyper-element.

Assignment of boundary conditions for labyrinth seals does not require any additional assumptions, meanwhile certain actions are needed for the balance holes. Namely, the flow rate should be uniformly smoothed along the ring that wraps the balance holes. This may lead to some uncertainty in disk cavity steam flow modeling, however, the axi-symmetric approach does not offer other solutions.

Heat transfer intensity between fluid in hyper-element channel and adjacent surfaces of meshed solid is determined with the help of appropriate equation for *Nu* number

$$Nu = A\,\mathrm{Re}^n\,\mathrm{Pr}^m\ldots \qquad (3)$$

Exit fluid temperature is simulated using entry fluid temperature, flow rate and heat exchange with adjacent solid surfaces.

Finally, it is worth to note that hyper-element of a channel preserves mass flow rate and energy conservation conditions.

A fragment of rotor-stator mesh with imaginary labyrinth seal and balance hole shown in Fig.1 illustrates the described technique. As a rule, solids are meshed by triangle elements as well as, where it is possible, by quadrilateral ones. The fluid was meshed by quadrilateral elements with boundary layers on disk and stator surfaces. Some of solid-fluid boundaries were unlinked just to set up a different type of conditions. The examples are flow inlet and convection on solid surfaces.

This approach makes possible to generate easy manageable mesh for a total system, which comprises only 213,126 nodes and 237,316 cells (Fig. 2). This allows to obtain the coupled solution of steam flow in 22 disk-rotor cavities and thermal state of rotor-stator system using regular modern personal computer.

Fig. 2 Model of the 11 stages-rotor and diaphragms of the hig-pressure steam turbine cylinder

3 Secondary Flow

3.1 Flow in the disk cavities

In engineering practice worldwide simple analytical solutions and experimental correlations for flow modeling in rotated disk and stationary stator system are used (see Shvetz, Dyban, 1974 and Boyko, Govorushchenko, 2002). However, this approach is valid only for classic designs with plain disk and stator and small flow rate. The flow through disk-rotor cavities in real turbines runs under more complicated conditions featuring fluid mixing in zones of balance holes and main-secondary steam mixing in turbine flow path. As it was emphasized in some papers (see Phadke, Owen, 1988 and unpublished Kapinos' investigation), design of disk sealing at the periphery directly determines flow pattern in the disk-stator system. This, in turn, directly influences ingress of main flow into the disk cavity. Such intricate flow patterns in the cavity require usage of powerful CFD packages to obtain more reliable solutions.

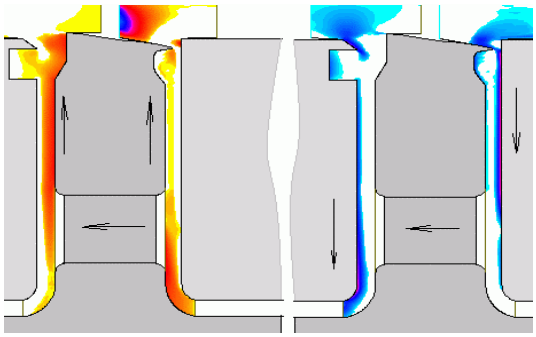

Fig. 3 Radial velocity in cavities around disk of the 4th stage. (a) - positive radial velocity in the range of 0 (blue) – 15 (red), m/s; (b) - negative velocity in the range of (-25) (blue) – 0 (light blue), m/s

Principally, design uniformity and physical proximity of disks and diaphragms defines similarity of steam flow behavior through the cavities. At the same time, it is worth to note that there are essential distinctions of real aerodynamics in the disk cavities and simplified pattern that is taken as a base for engineering methods of computation. In a framework of conventional methods, two opposite boundary layers should be formed at disk and stator. At this, flow motion along disk is centrifugal, while it is centripetal along stator.

In real practice, the flow pattern in and near the disk cavities features more complex nature caused by balance holes influence. There is one of the possible reasons: steam comes to the higher-pressure cavity (i.e. to the first one along steam motion) from main flow path, as well as from the diaphragm seal of the preceded stage. This results in the flows collision at the balance holes radius of location. Coming into the holes, steam acquires the velocity equal to rotational velocity of the disk, thereby intensifying pumping effect into the lower pressure cavity (i.e. into the second one along steam motion) and changing significantly the nature of flow pattern in a whole, and creation of the boundary layers in particular.

Following further along steam motion in the cavity, a different flow pattern is observed. Leaving the balance hole, steam spills in two directions: to periphery and to center, then entering the labyrinth seal (Fig. 3).

Because of centrifugal effect, steam is moving from center to periphery in both the higher (first) and lower (second) pressure cavities. Nevertheless, steam boundary layer on the left side of the disk (see Fig. 4) is driven off the wall by a steam cross flow from flow path.

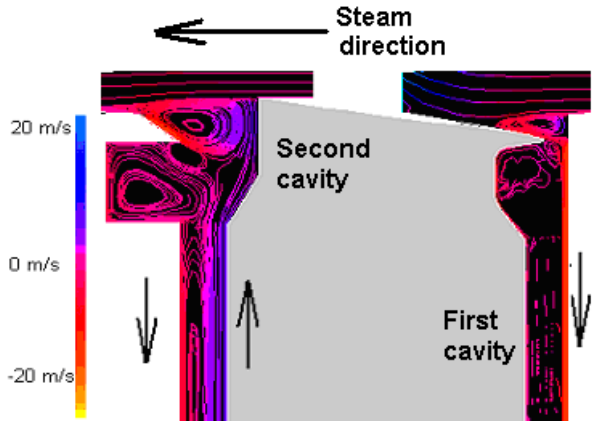

Fig. 4 Path lines colored by radial velocity

The well-formed boundary layer can be observed in the disk second cavity. This layer steadily runs from periphery to center along the stator's surface meanwhile along the disk surface it moves in opposite direction, i.e. from the balance hole.

Contrary to the second cavity, the flow in the first one is significantly destroyed by steam leakage from the flow path (Fig. 4). In this case, if simplified engineering methods are applied, it will result in significant loss of accuracy in centrifugal effect modeling and determining of heat exchange boundary conditions. Hence, search for new general dependencies that describe so tangled flow pattern will hardly lead to an acceptable solution. It is more likely that problem can be solved within the framework of coupled CFD analysis.

Steam leaking through the balance holes considerably equalizes pressure in the adjacent near-disk cavities. At the same time, the pressure in each cavity rises greatly along radius due to a pump effect. When steam moves from periphery to center, its twirling is much higher than for the motion in opposite direction. Due to this, the pump effect in the first cavity is greater than in the second one (Fig. 5).

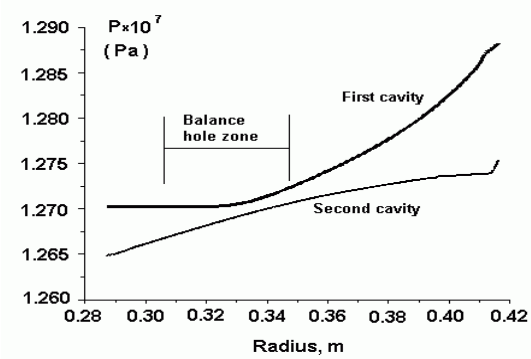

Fig. 5 Static pressure distribution in both near-to-disk cavities of the 4th stage

3.2 Flow rate

Current approach based on CFD modeling with controlled boundary conditions allows to simultaneously model 22 cavities preserving design and operational conditions. Turbulence is simulated following k-ε model.

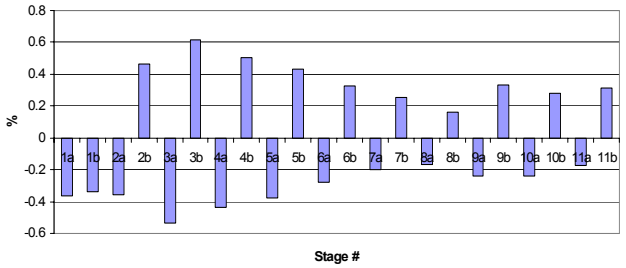

Fig. 6 Relative steam mass flow rate G_{leak}/G_{main} for suction (negative) and injection (positive) from/to flow path. Here 1a, 1b are the first and second cavities of the first disk, etc.

Flow analysis shows that in the majority of stages main steam passes through the first disk-rotor cavity (sealed between nozzles and blades) and comes into flow path from second cavity (sealed between blades and nozzles of the next stage). Both cavities of the first stage are filled by main steam flow, Fig. 6. High value of suction/injection flow rate takes place at the first stages and reaches 0.6% relatively to main steam flow rate (near 270 kg/s).

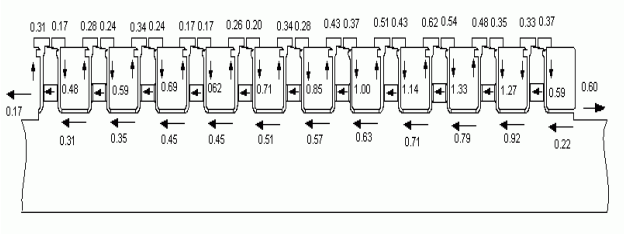

Fig. 7 Secondary steam relative mass flow rate vs. main steam flow

The flow rate decreases from stage to stage along flow path with maximum value near 1.33% through the balance hole of the third disk.

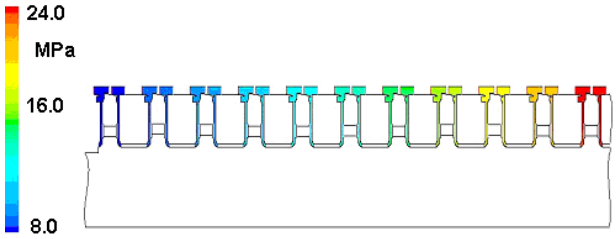

Fig. 8 Static pressure distribution of secondary steam

Steam leakages through the end exit seal is about 0.2% and through entry seal - 0.6% (Fig. 7).

3.3 Axial Force

Analysis of pressure behavior in the disk cavities reveals that 7 balance holes in each disk are sufficient to provide pressure balance on both sides of the disk (Fig. 8).

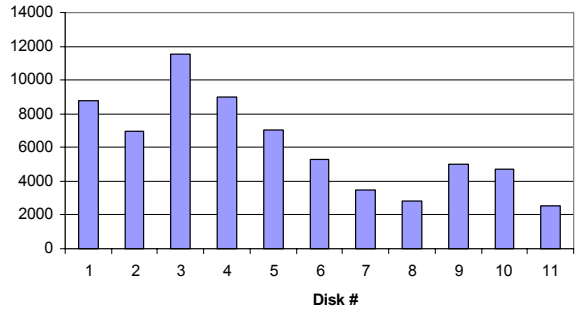

Fig. 9 Axial force (in Newtons)

As soon as the secondary steam pressure distribution is available, one can compute with sufficient accuracy a rotor axial force that is caused by secondary steam pressure drop on the disk's adjacent surfaces (Fig. 9). Maximum forces are exerted on the several first stages. Total force value for all stages is near 70,000 N.

3.4 Windage Losses

3.4.1 Windage Model of Labyrinth Seal

Friction heating in the disk-stator cavities is automatically simulated by CFD solver. At the same time, the hyper-elements can't contain heating generation option due to the lack of such kind of experimental correlations. Therefore, a CFD study of labyrinth seals was performed to obtain windage heating and power losses correlations.

The study includes numerous typical calculations for design of 11 knife labyrinth seal of the turbine with different operational and geometrical conditions.

In spite of variation of pressure drop, temperature, and seal sizes, there was revealed a certain general dependence, which reliably determines shaft energy losses. In particular, it was determined that a shaft linear velocity is a principle reason for shaft power loss, and the latter can be evaluated according to the following equation:

$$N = \sum_{i-1}^{z} \rho A_i (1-\beta_i^3) \frac{u_{\theta w}^{\ 3}}{2} + G(\beta_{outlet}^2 - \beta_{inlet}^2) \frac{u_{\theta w}^{\ 2}}{2} \qquad (4)$$

Here: z - number of knifes, $u_{\theta w}$ – shaft rotational velocity, $\beta = \frac{\overline{u}_\theta}{u_{\theta w}}$ - relative velocity of fluid (swirl factor), $\overline{u}_\theta$ - average steam swirl velocity, A - meridian cross section of a single labyrinth camera, G – mass flow rate.

The drop of total temperature was simulated as

$$\Delta T_{total} = \frac{N}{C_p G} \qquad (5)$$

The maximum of total temperature rise is about 5-6K at the high-pressure end labyrinth seal. This value is computed at the mean value of the swirl factor.

3.4.1 Windage Losses on the Disks

Viscous losses at the disk surface are generated at both sides of the disk, but they are higher in the second cavity since the boundary layer here is thicker and more steam should be accelerated by disk. The first cavity features a very thin boundary layer, and steam flow coming from the flow path with high tangential velocity transfers its energy to the disk. So, the losses could be small or even negative here.

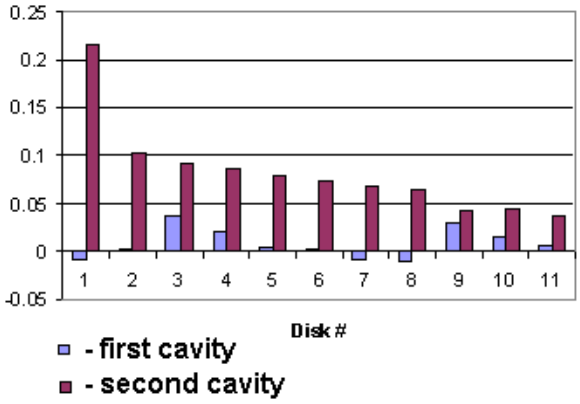

Fig. 10 Relative windage losses in disks – friction loss normalized by total frictional loss in all disks

The computation shows that total disk windage losses caused by friction around surface reaches over 55 kW with maximum in the first disk region (Fig. 10).

4 Thermal State

4.1 Steady State and Rotor's Elongation

The temperature of secondary steam gradually decreases along the turbine flow path due to steam-solid heat exchange that causes stator-rotor temperature decreasing in general. Steam inflow more or less compensates that drop but its influence is active within 2-3 next stages only (Fig. 11).

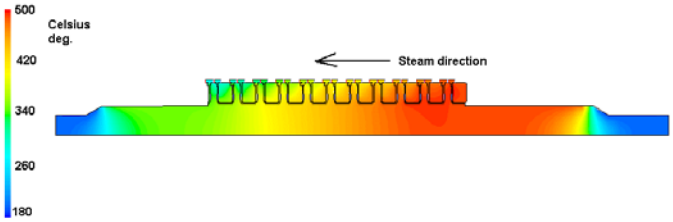

Fig. 11 Thermal state of rotor and diaphragms of large steam turbine

Shaft temperature is practically uniform in zones of terminal labyrinth seals but it slightly (3-5K) higher the steam temperature due to windage heating.

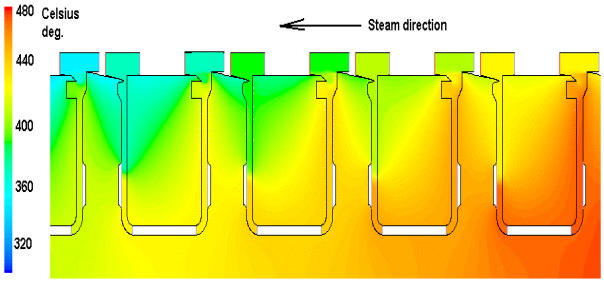

Fig. 12 Fragment of temperature distribution of rotor and diaphragms

Lower pressure end of the shaft is heated over 60-70 K comparing with steam exit temperature due to more preheated steam leakage from previous stages.

The temperature distribution across the system is determined by the steam secondary flows through the seals and balance holes. As a result, the shaft temperature turns out to be slightly above the temperature on the periphery of disks and diaphragms.

Maximum of rotor's axial elongation, taking into account its' thermal state, makes up to near 17.5 mm at exit end of the shaft. Value of elongation obtained under assumption that shaft and steam have the same temperature is near 15.5 mm (Fig. 13).

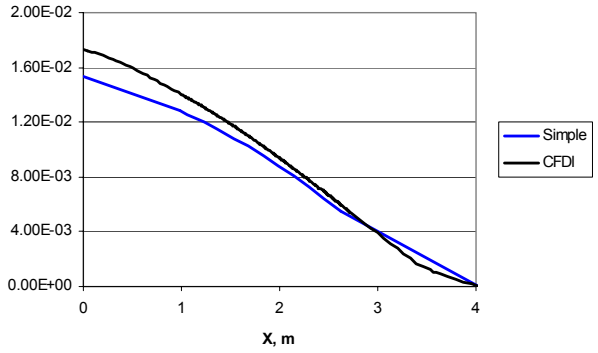

Fig. 13 Rotor's elongation from fix point, m. Simple – calculation based on assumption that temperature of the rotor equals to main steam temperature; CFDI – calculation based on rotor thermal state including heat exchange between main and secondary steam

Conclusions

Novel method that is based on the complete CFD analysis has been developed for solving coupled flow - thermal problem. It is found to be effective and highly informative when it was applied to the analysis of large thermodynamic systems.

The results of the study demonstrate successful analyses of secondary steam flow and thermal state of rotor and adjoined diaphragms in a large steam turbine. A full set of parameters for turbine's reliable operation has been obtained.

During the study the following additional analyses have been performed yielding:

- Rotor thermal elongation;
- Axial forces upon a thrust bearing at the account of pressure drops on both sides of disks;
- Frictional energy losses caused by disks and shaft rotation in labyrinth seals.

REFERENCES

Wilson, M., Pilbrow, R., Owen, J.M., 1997, "Flow and heat transfer in a preswirl rotor-stator system," ASME Journal of Turbomachinery, Vol. 119, pp.364-373

Pilbrow, R., Karabay, H., Wilson, M., Owen, J.M., 1999, "Heat transfer in a "cover-plate" preswirl rotating-disk system," ASME Journal of Turbomachinery, Vol. 121, pp.249-256

Shvetz, I.T., Dyban, E.P., 1974, "Air cooling of gas turbine parts", Kiev, 488 p. (in Russian)

Boyko, A.V., Govorushchenko, Yu.N., Yershov, S.V., Rusanov, A.V., Severin, S.D., 2002, "Aerodynamic computation and optimal projection of turbomachinery flow paths", Kharkov, NTU "KhPI", 356 p. (in Russian)

Phadke, U.P., Owen, J.M., 1988, "Aerodynamic aspect of the sealing of gas turbine rotor-stator system", Int. Journal of Heat and Fluid Flow, Vol. 9, 11, pp. 98-112

Matveev, Yu. Ya., Pustovalov, V.N., 1982, "Laminar viscous flow calculation between rotated disks", Fluid and Gas Mechanics, Proceeding of the Academic Science of USSR, 1, pp. 76-81 (in Russian)

Kapinos, V. M., 1966, "Convective heat transfer of turbulent flow between rotated disks in closed cavity", Proceeding of Higher School "Aviation technique", 1, pp. 132-129 (in Russian)

V. M., Matveev, Yu. Ya., Pustovalov, V.N., 1983, "Natural convection of unventilated cavities of steam turbines rotors", Thermal Engineering /Teploenergetika/, 8, pp. 36-39 (in Russian)